

# Design and analysis of a Sub-6 GHz antenna array with high gain for 5G mobile phone applications

Abderrahim Bellekhiri<sup>1</sup>, Noha Chahboun<sup>1</sup>, Jamal Zbitou<sup>1,2</sup>, Aziz Oukaira<sup>3</sup>, Yassin Laaziz<sup>1</sup>

<sup>1</sup>Laboratory of Information and Communication Technologies, National School of Applied Sciences of Tangier, University of Abdelmalek Essaadi, Tétouan, Morocco

<sup>2</sup>Laboratory of Information and Communication Technologies, National School of Applied Sciences of Tétouan, University of Abdelmalek Essaadi, Tétouan, Morocco

<sup>3</sup>Department of Engineering and Computer Science, University of Québec in Outaouais, Gatineau, Canada

## Article Info

### Article history:

Received Mar 29, 2024

Revised Jul 14, 2024

Accepted Aug 6, 2024

### Keywords:

5G

Antennas array

Directivity

Gain

Radiation pattern

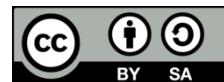
Reflection coefficient

Substrate

## ABSTRACT

In this paper, we designed, analyzed, and simulated a 32-element antenna array for the sub-6 GHz band. Each radiating element is a square patch on a Rogers RT5880 substrate, featuring a relative dielectric permittivity of 2.2, a low-loss tangent of 0.0009, and a thickness of 0.508 mm, measuring 28.1×28.1 mm<sup>2</sup>. Simulations were conducted using two electromagnetic solvers, advanced design system (ADS) and CST Microwave Studio, providing a comprehensive comparison of the results. To achieve a high balance between performance and antenna size, two 4×8 array antenna structures were designed. The simulations demonstrated excellent input impedance matching around 3.5 GHz for both configurations, with high gains of 20.5 dBi for the first and 18 dBi for the second configuration, along with directional radiation patterns. The dimensions were 315×576×0.578 mm<sup>3</sup> for the first configuration and 170×961×0.578 mm<sup>3</sup> for the second. These performance metrics make the proposed antenna arrays highly suitable for wireless communication technologies operating below 6 GHz, particularly for 5G mobile communications.

This is an open access article under the [CC BY-SA](https://creativecommons.org/licenses/by-sa/4.0/) license.



## Corresponding Author:

Abderrahim Bellekhiri

Laboratory of Information and Communication Technologies, National school of Applied Sciences of Tangier, Abdelmalek Essaadi University

Tetouan, Morocco

Email: abderrahim.bellekhiri@etu.uae.ac.ma

## 1. INTRODUCTION

Over the last few decades, wireless communication has undergone significant evolution driven by consumer demands for mobile broadband services [1], [2]. Traffic is expected to rise by 10 to 100 times between 2020 and 2030 necessitating innovative solutions to meet escalating demands while ensuring affordability and enhancing user experiences [3]. The annual report from Cisco [4] projected that by 2023, nearly two-thirds of the global population would have Internet access, with 5.3 billion users, constituting 66% of the world's population, compared to 3.9 billion in 2018 (51% of the world's population). With the use of fifth-generation (5G) mobile technology, intelligent networked communication environments may connect people, devices, data, applications, transportation systems, and entire cities. As 5G networks are deployed, the swift processing of massive data volumes, connectivity for numerous devices, and rapid data transmission become feasible [5], [6]. Massive machine-to-machine connections for industrial automation systems, virtual and augmented reality, remote medical services, 3D video, cloud computing and gaming, smart homes and buildings, and virtual and augmented reality are all supported by 5G technology. These enhanced services are

more capable than those offered by 3G and 4G networks [7].

Three separate spectrum bands are used for 5G (low-band, medium-band, and high-band). Every band has unique abilities: the low band (from 600 to 700 MHz) delivers more coverage but slightly slower speed, the mid-band (from 3 to 5 GHz) provides a balance of both, and the high band (from 24 to 100 GHz) offers faster speed but a narrower coverage area [8]. High-frequency waves like mm-waves can only travel a relatively limited distance due to greater atmospheric attenuations [9]. Implementing mm-wave devices is expensive due to higher path loss, requiring denser cell deployment [10]. In response, leveraging sub-6 GHz bands offers an attractive alternative, particularly by leveraging existing 4G long-term evolution (LTE) systems. Sub-6 GHz 5G transmissions are appropriate for both urban and rural settings since they can provide high data speeds over a range of distances. As a result, significant research efforts are now directed towards the sub-6 GHz band, predominantly deployed worldwide in the 3.3 to 3.8 GHz frequency range, as indicated in Table 1 [11].

The 5G antennas need to have high gain and improved directivity in order to overcome the route loss. Many attempts have been made to enhance the performance of antenna designs for 5G applications; the difficulty lies in creating an antenna that is compact, low-cost, and extremely efficient. All the previously suggested antennas in [12]–[15] exhibit modest gains for the sub-6 GHz 5G frequency spectrum, which are not aligned with the desired antenna performance for this frequency band. Specifically, an ideal antenna for this spectrum should be low-profile, broadband, and high gain [16]. One of the main techniques to address this issue is multi-element array configuration. With an electrically down-tilted, six-element dual-polarized array, a peak gain of 16.8 dBi is achieved and measured in [17]. Six antenna elements are used in this process, and a radio frequency phase shifting module (RFPSM) built using vector modulators is the result. With a new frequency-selective surface (FSS) reflector, the designed antenna configuration of a 1×4 rectangular microstrip array antenna produced semi-stable gains of 12.4 dBi at 4.1 GHz and 11.4 dBi at 3.5 GHz [18]. In [19], [20], higher gain is reported; for example, the measured realized gains of the 1×4 antenna array are 8.34±0.39 dBi and 15.1±0.4 dBi at 3.28–3.71 GHz and 4.8–5.18 GHz respectively.

The main objective of this work is to construct a small antenna array with enhanced gain at 3.5 GHz for fifth generation (5G) sub-6 GHz wireless communication systems. For this purpose, we designed a 4×8 antenna array containing 32 radiating squared elements. Two different configurations were considered to build this structure: parallel and squared array arrangements. Both configurations made it possible to obtain quite interesting results in terms of compactness, gain and directivity, with an advantage for the squared arrangement which has limited the presence of side-bands around 3.5 GHz. To feed the proposed antenna array we adopt both series and parallel feeding techniques due to their simplicity of implementation. These techniques can be integrated on the same network layer, optimizing weight, thickness, and overall antenna costs. The designed antennas were simulated and enhanced by the use of the moment method-based advanced design system (ADS) and the finite integration technique-based CST microwave studio.

Table 1. The distribution of 5G sub-6 GHz spectrum across different countries

Countries	3 to 4 GHz range	4 to 5 GHz range	5 to 7 GHz range
United States	3.45-3.7, 3.7-3.98	3.49-4.99	5.9-7.1
Canada	3.47-3.65, 3.65-4.0		
Korea	3.4-3.7, 3.7-4.0		26.5–28.1
India	3.4-3.6		26/28
Australia	3.5		27.5–28.35
Italy	3.6-3.8		
Japan	3.6-4.1	4.5-4.9	
China	3.3-3.6	4.5-5	

## 2. PROCEDURES FOR DESIGN

### 2.1. The standard square microstrip patch antenna's design

Using a microstrip line as the feed, we first designed a square microstrip patch antenna that would operate at 3.5 GHz. The equations (1) and (2) were used to calculate the patch's dimensions in the first step [18]:

$$L = \frac{1}{2f_r \sqrt{\epsilon_{reff} \sqrt{\mu_0 \epsilon_0}}} - 2\Delta L \quad (1)$$

$$W = \frac{1}{2f_r \sqrt{\mu_0 \epsilon_0} \sqrt{\epsilon_r + 1}} \quad (2)$$

where  $f_r$ : resonant frequency,  $\mu_0$  and  $\varepsilon_0$ : permeability and permittivity in free space,  $\varepsilon_r$ : relative dielectric permittivity, and  $\Delta L$ : the length of the patch length around the slots.

The effective dielectric permittivity ( $\varepsilon_{reff}$ ) can be determined using (3).

$$\varepsilon_{reff} = \frac{\varepsilon_r + 1}{2} + \frac{\varepsilon_r - 1}{2} \left(1 + 12 \frac{h}{W}\right)^{-\frac{1}{2}} \quad (3)$$

'h' is the height of the substrate and  $\Delta L$  may be computed by using (4).

$$\frac{\Delta L}{h} = 0.412 \frac{(\varepsilon_r + 0.3) \left(\frac{W}{h} + 0.264\right)}{(\varepsilon_{reff} - 0.258) \left(\frac{W}{h} + 0.8\right)} \quad (4)$$

The feed widths of different impedances can be calculated using the (5).

$$\frac{w_f}{h} = \left\{ \begin{array}{l} \frac{8e^A}{e^{2A} - 2}, \quad \frac{w_0}{h} \leq 2 \\ \frac{2}{\mu} \left\{ B - 1 - \ln(2B - 1) + \frac{\varepsilon_r - 1}{2\varepsilon_r} \left[ \ln(B - 1) + 0.39 - \frac{0.61}{\varepsilon_r} \right] \right\}, \quad \frac{w_0}{h} \geq 2 \end{array} \right\} \quad (5)$$

$$\text{where } A = \frac{Z_A}{60} \sqrt{\frac{\varepsilon_r + 1}{2}} + \frac{\varepsilon_r + 1}{\varepsilon_r - 1} \left(0.23 + \frac{0.11}{\varepsilon_r}\right); \quad B = \frac{377\pi}{2Z_A \sqrt{\varepsilon_r}}$$

Following the verification of the patch element's size, which enabled a 3.5 GHz resonance, we connected the quarter wave to match the input impedance of 50 Ohm. The patch antenna is 28.1×28.1 mm<sup>2</sup>, has a height of 0.508 mm, a loss tangent of  $\tan(\delta) = 0.0009$ , and is printed on a Rogers RT 5880 substrate. Table 2 displays the improved square antenna specifications.

Table 2. The 3.5 GHz optimal parameters of a traditional patch antenna

Parameter	Value (mm)	Parameter	Value (mm)
$W_p$	28.1	$W_f$	0.41
$L_p$	28.1	$L_f$	16.28
$W_s$	55	$h$	0.508
$L_s$	60	$t$	0.035

## 2.2. Creating a 4x8 antenna array design-first configuration

In the first step, the conventional square antenna described above is used to construct a 2×4 antenna array composed of 8 elements, as shown in Figure 1. The spacing between two patch radiators is set to  $\lambda_g/2$  in order to prevent mutual coupling between patches caused by proximity while building a linear array with beamforming capability [21]. Furthermore, for the radiator patch, a quarter-wavelength transformer is used as a feeder, and a power divider is employed to feed each patch antenna with equal input power. The designed 2×4 antenna array includes 4×1 subarrays which are fed in parallel. Signal distribution across all linear antenna subarrays has previously been accomplished using a parallel feeding network made up of power dividers [22].

The spacing between the sub-arrays is  $W_g$  and the guided wavelength is calculated according to (6); at 3.5 GHz,  $\lambda_g = 57.588$  mm. Additionally, quarter-wave transformers were used to match the impedance to the power dividers. The impedance of quarter-wave transformers is given by (7), where  $Z_C$  is the line input impedance, and  $Z_A$  is the characteristic impedance. The values of  $Z_0$  and  $Z_A$  are respectively 50 and 169  $\Omega$ . Moreover, the 1×4 sub-arrays are fed in parallel using microstrip lines of characteristic impedances 100, 70.7 and 50  $\Omega$ .

$$\lambda_g = \frac{3 \times 10^8}{f_r \sqrt{\varepsilon_{reff}}} \quad (6)$$

$$Z = \sqrt{Z_C Z_A} \quad (7)$$

The parameter  $W_g$  is optimized to minimize performance degrading by mutual coupling effect. The optimization is achieved by simulating different values of  $W_g$  corresponding to fractions of the guided wavelength at 3.5 GHz ( $W_g = a \times \lambda_g$ ;  $a = \{0.3; 0.4; 0.5; 0.6; 0.7\}$ ). The optimal value of  $W_g$  is found to be  $0.7 \times \lambda_g$ , resulting in a satisfactory return loss, gain, and efficiency as shown in Figures 2 and 3.

In the second step, we constructed a higher-order array of 32 elements by arranging four of the previously discussed  $4 \times 2$  arrays in parallel. The simulations result for this antenna are presented in Figure 4. We achieved good input impedance matching at 3.5 GHz, as shown in Figure 4(a), along with multiband behavior in Figure 4(a). Additionally, Figures 4(b) and (c) show the antenna's high gain of 20.5 dBi and directed radiation pattern, respectively.

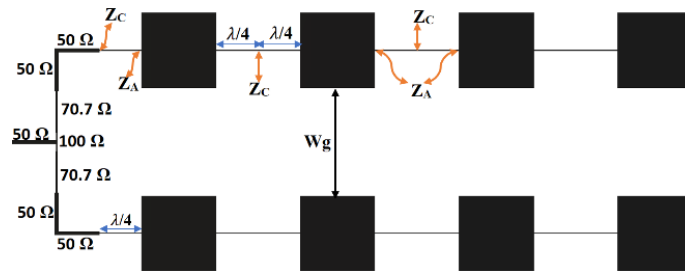


Figure 1.  $2 \times 4$  Antenna array geometry

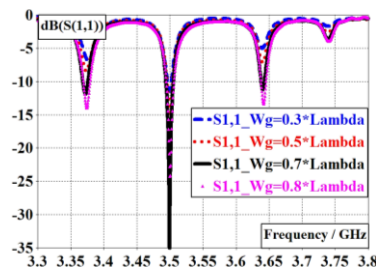


Figure 2. Return loss

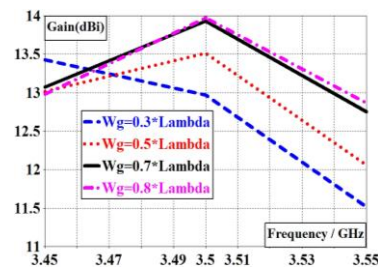
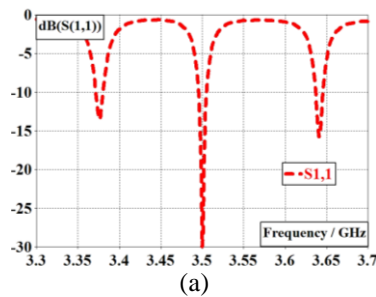
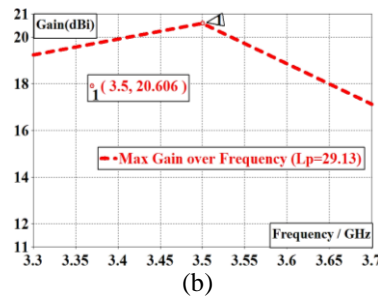


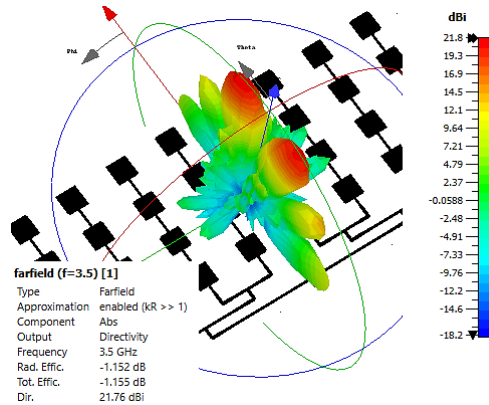
Figure 3. Gain versus frequency



(a)



(b)



(c)

Figure 4. Simulation results for the first configuration of the  $4 \times 8$  array antenna (a) return loss, (b) gain versus frequency, and (c) antenna geometry and 3D radiation pattern

Figure 5 provides a comparison of the results obtained for this antenna using two different solvers: CST-MW and ADS4. Figure 5(a) shows good agreement of the return loss obtained by the two solvers. As shown in Figure 5(b), the gain and radiation pattern produced by the ADS solver, allowing for comparison with the corresponding results obtained previously with CST-MW, showing excellent matching.

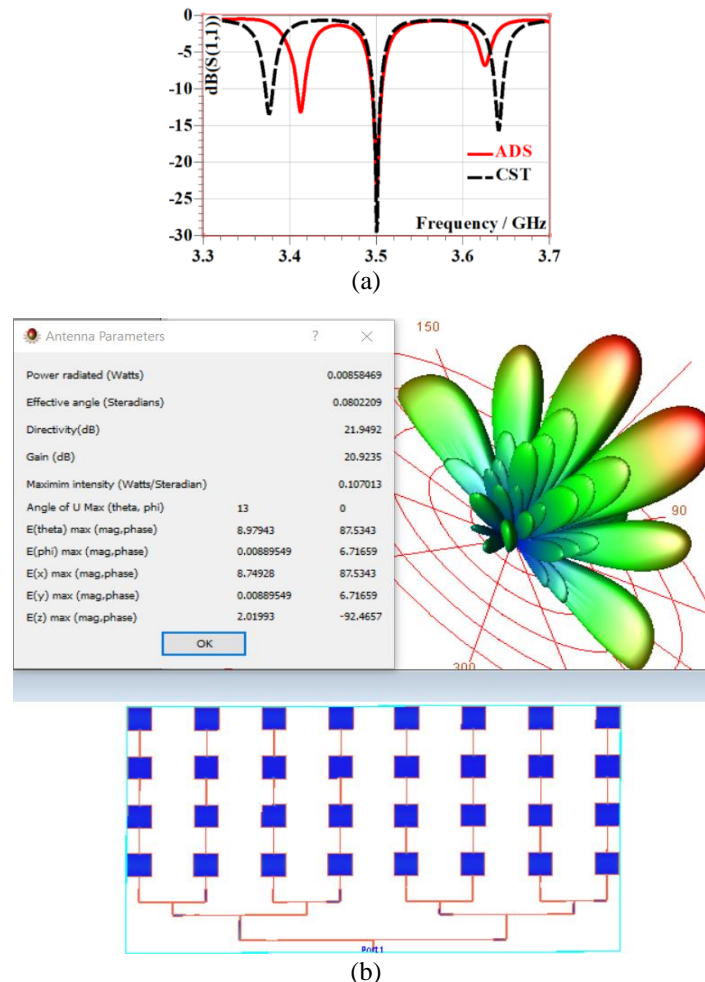


Figure 5. Results obtained with different solvers for the first configuration of the  $4 \times 8$  array antenna: (a) return loss versus frequency using ADS and CST-MW and (b) gain and 3D radiation pattern using ADS

### 2.3. Design of a $4 \times 8$ antenna array-second configuration

To miniaturize the antenna dimensions and eliminate the sideband effect, we modified the shape of the antenna array while maintaining the conventional microstrip patch antenna dimensions. Figure 6 illustrates the geometry and performance of the new squared sub-array antenna consisting of 4 radiating elements. Figure 6(a) provides the optimized characteristic impedances for the validated sub-array. Simulations confirmed good input impedance matching at 3.5 GHz in Figure 6(b), with a directional radiation pattern in Figure 6(c), and a gain of 9.58 dBi in Figure 6(d).

To enhance antenna gain, we designed a 16-element antenna array by combining 4 sub-arrays. The geometry and performance results for this high-order array are shown in Figure 7. Figure 7(a) illustrates the spatial arrangement and interconnections of the 16-element array. Simulations in Figure 7(b) indicate favorable impedance matching around 3.5 GHz, with a return loss of -27 dB. Figure 7(c) presents improved radiation patterns, while Figure 7(d) shows significant gain enhancement at 3.5 GHz, peaking at 15.12 dBi.

For the 32-element antenna array, 8 sub-arrays were integrated. The geometry and performance characteristics of this antenna are presented in Figure 8. The simulations reveal an enhancement in the reflection coefficient, with a single resonant frequency centered at 3.5 GHz, as shown in Figure 8(a), and an achieved gain of 18 dBi as illustrated in Figure 8(b). Figure 8(c) gives the radiation pattern obtained with the 32-element antenna array which shows a directional behavior.

In Figure 9, we compared the simulation results of the second configuration 4×8 array antenna, obtained using two simulators: CST-MW and ADS. As shown in Figure 9(a), there is a strong agreement between both solvers regarding the variations in the reflection coefficient and the resonant frequency. Additionally, the radiation pattern obtained with ADS in Figure 9(b) closely matches that observed with CST-MW in Figure 8(c), and the gain values obtained from both simulations are very close.

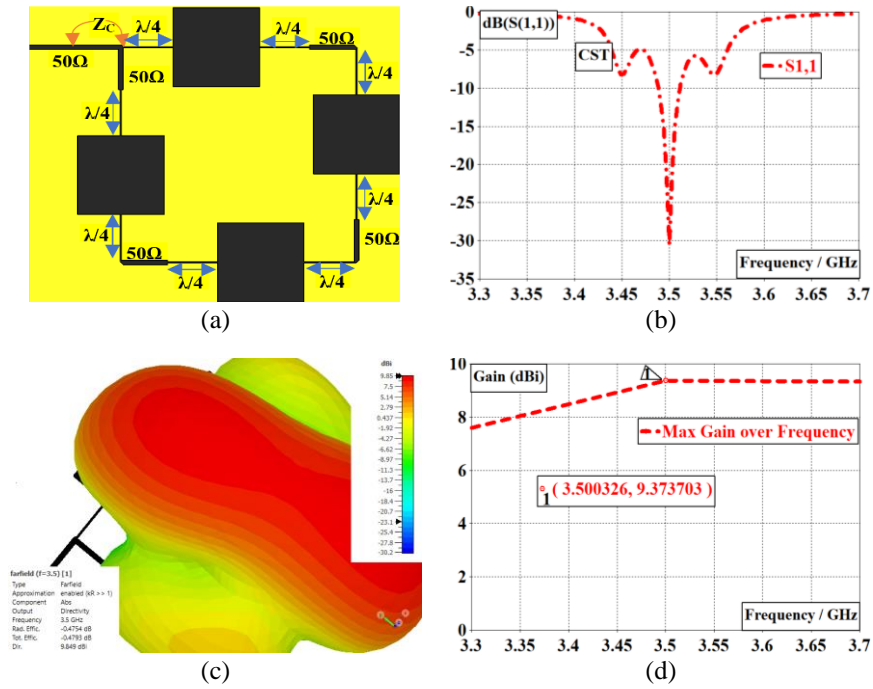


Figure 6. Geometry and simulation results for the 2<sup>nd</sup> configuration of the 1×4 sub-array: (a) geometry of the 1×4 radiating elements, (b) return loss, (c) 3D radiation pattern, and (d) gain versus frequency

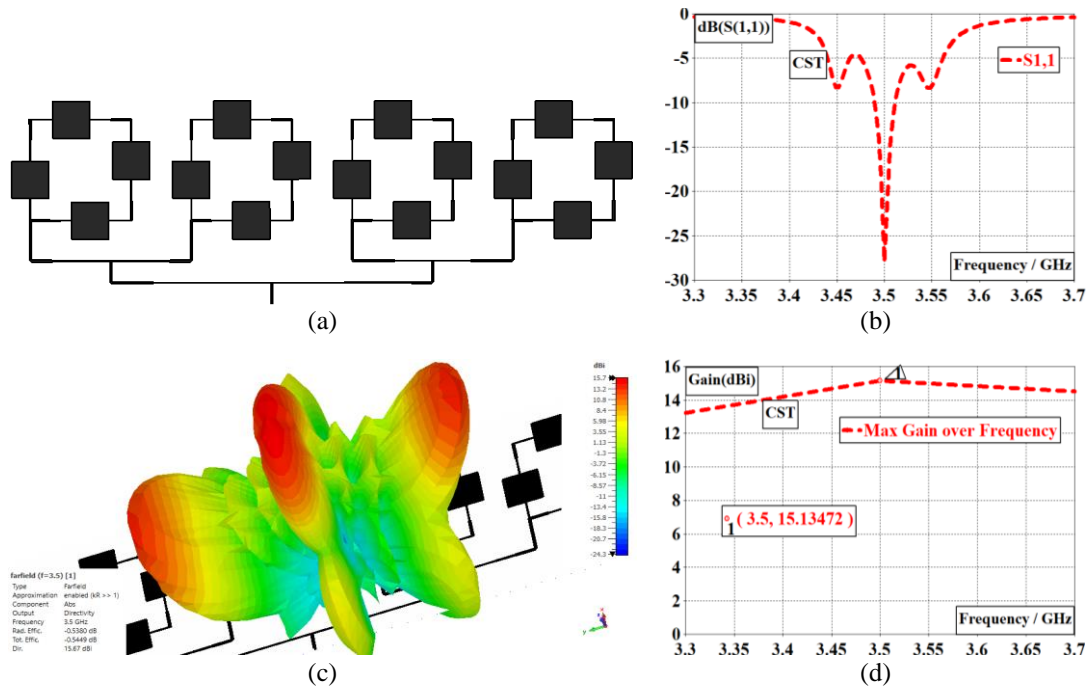


Figure 7. Geometry and simulation results for the second configuration of the 16 elements array antenna: (a) antenna geometry, (b) return loss, (c) 3D radiation pattern, and (d) gain versus frequency

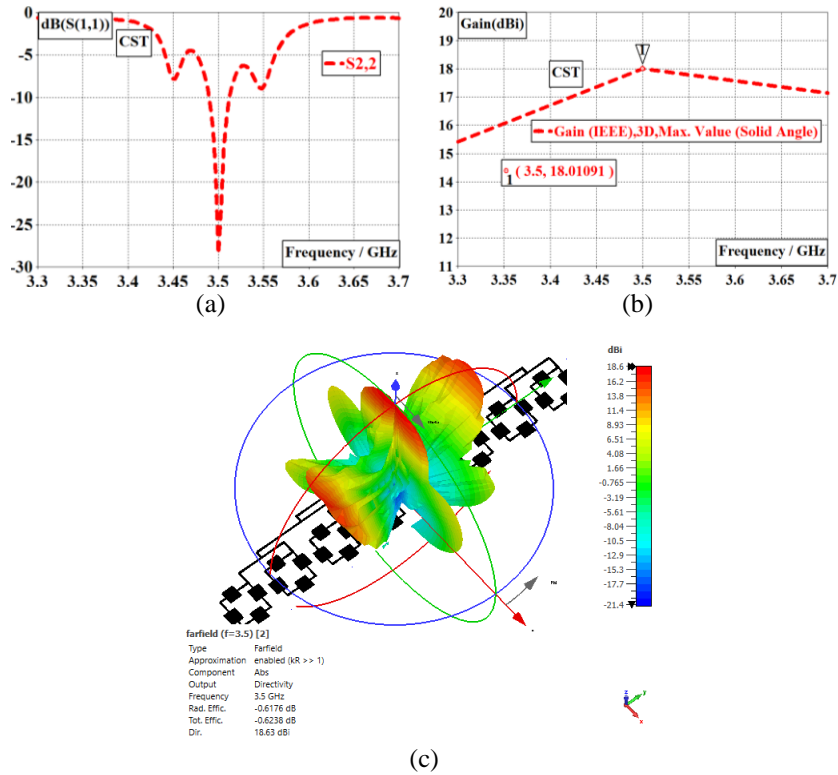


Figure 8. Geometry and simulation results for the 2<sup>nd</sup> configuration of the 4x8 array antenna: (a) return loss, (b) gain versus frequency, and (c) 3D radiation pattern

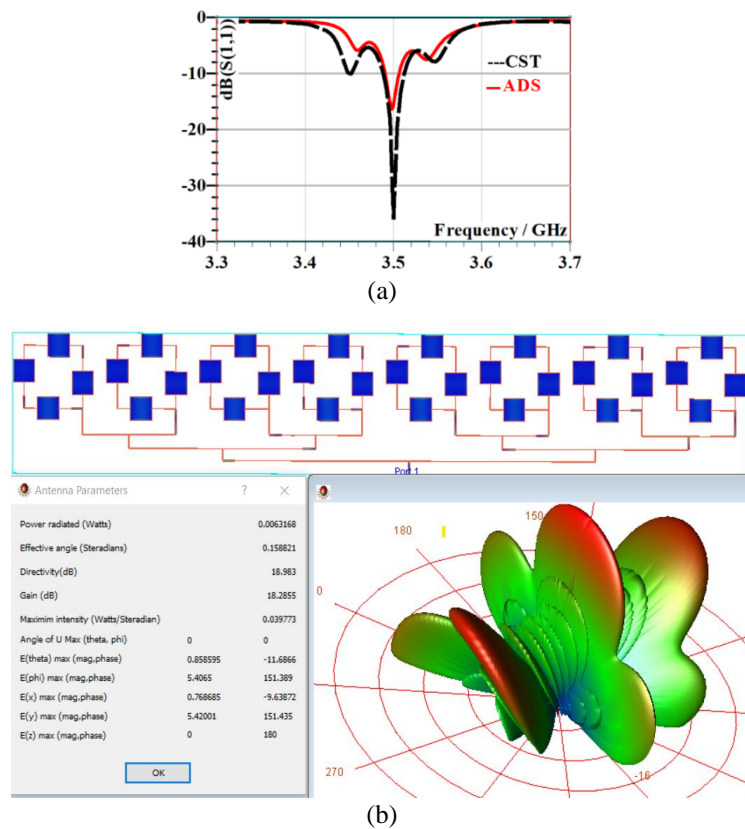


Figure 9. ADS solver comparison for the 2<sup>nd</sup> configuration of the 4x8 array antenna: (a) return loss vs frequency and (b) gain, and 3D radiation pattern

## 2.4. Results summary

This study focused on designing array antennas with optimal performance for the 5G sub-6 GHz band. To achieve high gain, two configurations of a 4×8 antenna were designed and simulated using two distinct solvers to confirm the results. The compactness was maximized through optimization of the spacing between the radiating elements, ensuring minimal performance degradation. Both developed antennas demonstrated high performance, with gains of 20.5 dBi for the first configuration and 18 dBi for the second. However, the second configuration offers greater compactness by utilizing less substrate surface area (1633.7 cm<sup>2</sup> vs 1814.4 cm<sup>2</sup>) and effectively mitigates the sideband effects that impact the first configuration.

Table 3 presents a comparative analysis of the array antennas developed in this study against other sub-6 GHz antennas from published research. Considering the lowest resonant frequency of 3.5 GHz for our antennas and the trend of increasing patch dimensions with decreasing frequency, both configurations ensure excellent performance within a compact size. This makes them highly suitable for potential applications in 5G networks, where efficient use of space and high performance are critical. Additionally, the optimized design guarantees robust input impedance matching and a directional radiation pattern, essential for reliable and high-quality wireless communication in 5G systems.

Table 3. Performance comparison between the antenna array proposed in this work and some state-of-the-art array antenna structures

References	Antenna size (mm <sup>2</sup> )	No. of element	Frequency (GHz)	$G_{max}$ (dBi)
[23]	344×344×63	4×4	4.3	8.6
[18]	166×66×1.6	1×4	4.1	12.4
[24]	226.8×148.2×8	3×6	4.35	16
[25]	170×60×8	1×4	3.6	5
[26]	165×235×0.787	1×8	5.57	12.4
[27]	120×85×3.255	2×2	4.148	12.1dB without reflection
1st conf.	315×576×0.578	4×8	3.5	20.5
2nd conf.	170×961×0.578	4×8	3.5	18

## 3. CONCLUSION

Designing antennas that balance compactness and high performance is challenging. In this work, we detailed the design process of a 32-element array antenna suitable for 5G mobile phone applications, operating at 3.5 GHz. The antenna design meticulously addressed the issue of performance degradation due to mutual coupling between elements while maximizing compactness.

Two antenna array configurations were proposed and validated through simulations using two different electromagnetic solvers. The first configuration demonstrated good performance in terms of radiation pattern, input impedance matching, and a gain of 20.5 dBi, but it exhibited sidebands around 3.5 GHz. The second configuration effectively addressed this issue and offered better compactness, with a slightly lower gain of 18 dBi, which remains quite high. Compared to other antenna structures in the literature, both configurations exhibit commendable performance, making them suitable for potential use in 5G mobile networks.

## REFERENCES





- [1] T. Nagaraj and R. K. Channarayappa, "An efficient security framework for intrusion detection and prevention in internet-of-things using machine learning technique," *International Journal of Electrical and Computer Engineering*, vol. 14, no. 2, pp. 2313–2321, Apr. 2024, doi: 10.11591/ijece.v14i2.pp2313-2321.
- [2] N. Nisha, N. S. Gill, and P. Gulia, "A review on machine learning based intrusion detection system for internet of things enabled environment," *International Journal of Electrical and Computer Engineering*, vol. 14, no. 2, pp. 1890–1898, Apr. 2024, doi: 10.11591/ijece.v14i2.pp1890-1898.
- [3] S. Iffat Naqvi and N. Hussain, "Antennas for 5G and 6G communications," *5G and 6G Enhanced Broadband Communications [Working Title]*, 2022, doi: 10.5772/intechopen.105497.
- [4] Cisco, "Cisco annual internet report (2018-2023)," Cisco, 2020. <https://www.cisco.com/c/en/us/solutions/collateral/executive-perspectives/annual-internet-report/white-paper-c11-741490.html> (accessed Apr. 05, 2023).
- [5] K. Shakir Muttair, A. Z. Ghazi Zahid, O. Ahmed Shareef, A. M. Qasim Kamil, and M. Farhan Mosleh, "A novel design of wide and multi-bands 2×2 multiple-input multiple-output antenna for 5G mm-wave applications," *International Journal of Electrical and Computer Engineering*, vol. 12, no. 4, pp. 3882–3890, Aug. 2022, doi: 10.11591/ijece.v12i4.pp3882-3890.
- [6] C. R. Storck and F. Duarte-Figueiredo, "A survey of 5G technology evolution, standards, and infrastructure associated with vehicle-to-everything communications by internet of vehicles," *IEEE Access*, vol. 8, pp. 117593–117614, 2020, doi: 10.1109/ACCESS.2020.3004779.
- [7] S. Kumar, A. S. Dixit, R. R. Malekar, H. D. Raut, and L. K. Shevada, "Fifth generation antennas: a comprehensive review of design and performance enhancement techniques," *IEEE Access*, vol. 8, pp. 163568–163593, 2020, doi: 10.1109/ACCESS.2020.3020952.






- [8] C. Y. D. Sim, H. Y. Liu, and C. J. Huang, "Wideband MIMO antenna array design for future mobile devices operating in the 5G NR frequency bands n77/n78/n79 and LTE band 46," *IEEE Antennas and Wireless Propagation Letters*, vol. 19, no. 1, pp. 74–78, 2020, doi: 10.1109/LAWP.2019.2953334.
- [9] I. Shayea, T. Abd Rahman, M. Hadri Azmi, and M. R. Islam, "Real measurement study for rain rate and rain attenuation conducted over 26 GHz microwave 5G link system in Malaysia," *IEEE Access*, vol. 6, pp. 19044–19064, 2018, doi: 10.1109/ACCESS.2018.2810855.
- [10] L. Hu *et al.*, "A wideband high-efficiency GaN MMIC power amplifier for sub-6-GHz applications," *Micromachines*, vol. 13, no. 5, 2022, doi: 10.3390/mi13050793.
- [11] M. A. Sufian, N. Hussain, H. Askari, S. G. Park, K. S. Shin, and N. Kim, "Isolation enhancement of a metasurface-based MIMO antenna using slots and shorting Pins," *IEEE Access*, vol. 9, pp. 73533–73543, 2021, doi: 10.1109/ACCESS.2021.3079965.
- [12] A. Desai, R. Patel, T. Upadhyaya, H. Kaushal, and V. Dhasarathan, "Multiband inverted E and U shaped compact antenna for Digital broadcasting, wireless, and sub 6 GHz 5G applications," *AEU - International Journal of Electronics and Communications*, vol. 123, 2020, doi: 10.1016/j.aeue.2020.153296.
- [13] H. W. Lai and H. Wong, "Substrate integrated magneto-electric dipole antenna for 5G Wi-Fi," *IEEE Transactions on Antennas and Propagation*, vol. 63, no. 2, pp. 870–874, 2015, doi: 10.1109/TAP.2014.2384015.
- [14] S. Ullah, I. Ahmad, Y. Raheem, S. Ullah, T. Ahmad, and U. Habib, "Hexagonal shaped CPW Feed based frequency reconfigurable antenna for WLAN and Sub-6 GHz 5G applications," in *2020 International Conference on Emerging Trends in Smart Technologies, ICETST 2020*, 2020, pp. 1–4, doi: 10.1109/ICETST49965.2020.9080688.
- [15] A. K. Vallappil, B. A. Khawaja, M. K. A. Rahim, M. N. Iqbal, and H. T. Chattha, "Metamaterial-inspired electrically compact triangular antennas loaded with CSRR and  $3 \times 3$  cross-slots for 5G indoor distributed antenna systems," *Micromachines*, vol. 13, no. 2, 2022, doi: 10.3390/mi13020198.
- [16] K. Shafique, B. A. Khawaja, F. Sabir, S. Qazi, and M. Mustaqim, "Internet of things (IoT) for next-generation smart systems: a review of current challenges, future trends and prospects for emerging 5G-IoT Scenarios," *IEEE Access*, vol. 8, pp. 23022–23040, 2020, doi: 10.1109/ACCESS.2020.2970118.
- [17] H. Jin, L. Zhu, H. Zou, Y. Luo, S. Xu, and G. Yang, "A wideband dual-polarized antenna and its array with electrically Downtilt function for 5G Sub-6 GHz communication applications," *IEEE Access*, vol. 8, pp. 7672–7681, 2020, doi: 10.1109/ACCESS.2019.2959378.
- [18] H. Alwareth, I. M. Ibrahim, Z. Zakaria, A. J. A. Al-Gburi, S. Ahmed, and Z. A. Nasser, "A wideband high-gain microstrip array antenna integrated with frequency-selective surface for sub-6 GHz 5G applications," *Micromachines*, vol. 13, no. 8, 2022, doi: 10.3390/mi13081215.
- [19] Y. Li, Z. Zhao, Z. Tang, and Y. Yin, "Differentially fed, dual-band dual-polarized filtering antenna with high selectivity for 5G Sub-6 GHz base station applications," *IEEE Transactions on Antennas and Propagation*, vol. 68, no. 4, pp. 3231–3236, Apr. 2020, doi: 10.1109/TAP.2019.2957720.
- [20] R. Y. Khattak, Q. Ahmed, S. Shoaib, and M. Hafeez, "Array antenna for wireless access points and futuristic healthcare devices," *Electronics (Switzerland)*, vol. 11, no. 8, 2022, doi: 10.3390/electronics11081226.
- [21] N. L. Nguyen and V. Y. Vu, "Gain enhancement for MIMO antenna using metamaterial structure," *International Journal of Microwave and Wireless Technologies*, vol. 11, no. 8, pp. 851–862, 2019, doi: 10.1017/S175907871900059X.
- [22] K. K. M. Cheng and C. Law, "A novel approach to the design and implementation of dual-band power divider," *IEEE Transactions on Microwave Theory and Techniques*, vol. 56, no. 2, pp. 487–492, 2008, doi: 10.1109/TMTT.2007.914629.
- [23] Y. Zhu, Y. Chen, and S. Yang, "Integration of 5G rectangular MIMO antenna array and GSM antenna for dual-band base station applications," *IEEE Access*, vol. 8, pp. 63175–63187, 2020, doi: 10.1109/ACCESS.2020.2984246.
- [24] M. Temiz, E. Alsusa, L. Danoon, and Y. Zhang, "On the impact of antenna array geometry on indoor wideband massive MIMO networks," *IEEE Transactions on Antennas and Propagation*, vol. 69, no. 1, pp. 406–416, 2021, doi: 10.1109/TAP.2020.3008662.
- [25] M. Li, X. Chen, A. Zhang, W. Fan, and A. A. Kishk, "Split-ring resonator-loaded baffles for decoupling of dual-polarized base station array," *IEEE Antennas and Wireless Propagation Letters*, vol. 19, no. 10, pp. 1828–1832, 2020, doi: 10.1109/LAWP.2020.3020855.
- [26] J. Khan, S. Ullah, F. A. Tahir, F. Tubbal, and R. Raad, "A sub-6 GHz MIMO antenna array for 5g wireless terminals," *Electronics (Switzerland)*, vol. 10, no. 24, 2021, doi: 10.3390/electronics10243062.
- [27] C. Apriono, B. P. A. Mahatmanto, and F. H. Juwono, "Rectangular microstrip array feed antenna for c-band satellite communications: preliminary results," *Remote Sensing*, vol. 15, no. 4, 2023, doi: 10.3390/rs15041126.

## BIOGRAPHIES OF AUTHORS






**Abderrahim Bellekhiri**     was born in Bir Jdid, Morocco, in October 1984. He obtained a master's degree in networks and telecommunications from the Faculty of Sciences of El Jadida, Chouaib Doukkali University, Morocco, in 2011. He is currently a Ph.D. student at the National School of Applied Sciences in Tangier, Morocco, part of Abdelmalek Essaadi University. His research interests focus on the design and analysis of periodic structure-based (MTM) RF antennas for 5G. He can be contacted at [abderrahim.bellekhiri@etu.uae.ac.ma](mailto:abderrahim.bellekhiri@etu.uae.ac.ma).






**Noha Chahboun**    was born in Chefchaouen, Morocco, in 1969. She obtained her postgraduate doctorate in physics in 1994 from Cadi Ayyad University in Marrakech, Morocco, where she worked on ternary semiconductor thin films for optoelectronic devices. She has been an associate professor since September 1995, initially at the Faculty of Sciences of Marrakech and, since July 1999, at the National School of Applied Sciences in Tangier, Morocco, part of Abdelmalek Essaadi University. Her current research focuses on the design of antennas based on metamaterials and metasurfaces, particularly for 5G mobile communications. She can be contacted at [n.chahboun@uae.ac.ma](mailto:n.chahboun@uae.ac.ma).






**Jamal Zbitou**    was born in Fes, Morocco, in June 1976. He received his Ph.D. degree in electronics from Polytech Nantes, University of Nantes, France, in 2005. He is currently a Full Professor of Electronics and Telecommunications at ENSA of Tetuán, part of Abdelmalek Essaadi University, and a full member of the Laboratory of Information and Communication Technologies (LabTIC). His research involves the design of hybrid, monolithic, active, and passive microwave electronic circuits. He can be contacted at [j.zbitou@uae.ac.ma](mailto:j.zbitou@uae.ac.ma).



**Aziz Oukaira**    received a Ph.D. degree in electrical engineering from UQO (the University of Québec in Outaouais), QC, Canada, in 2020. He is currently a postdoctoral fellow with the Polystim Neurotechnologies Laboratory, Ecole Polytechnique de Montreal, Montreal, QC, Canada. His primary interest research is oriented toward thermal management, rapid prototyping on FPGA, MEMS, microelectronics, thermal aspects in VLSI microsystems, and parallel architecture platforms for embedded systems. His secondary research area is related to designing robust and user-friendly wearable systems for health monitoring using textile sensors, printed and flexible circuits (PFC), and other types of sensors. Email: [aoukaira@uottawa.ca](mailto:aoukaira@uottawa.ca).



**Yassin Laaziz**    was born in 1966. He obtained his postgraduate doctorate in physics from Abdelmalek Essaadi University (UAE) in Tetouan, Morocco, in 1992, followed by a Doctorate of State in physics from Cadi Ayyad University (UCA) in Marrakech, Morocco, in 1999. From 1992 to 1999, he served as an assistant professor at the Faculty of Sciences and Techniques in Marrakech. Subsequently, he joined the National School of Applied Sciences in Tangier, Morocco (UAE), where he held positions as the head of the Telecommunications and Electronics Department and coordinator of the Telecommunications and Networks Engineering program. He also directed two master's programs: networks and systems and telecommunications and embedded systems. He is a founding member of the Laboratory of Information and Communication Technologies (LabTIC), where he has been the director since 2017. His current research focuses on wireless communication systems, RF devices, and artificial intelligence systems. He can be contacted at [ylaaziz@uae.ac.ma](mailto:ylaaziz@uae.ac.ma).